water

MDPI

Article

Assessment of Three Long-Term Gridded Climate Products for Hydro-Climatic Simulations in Tropical River Basins

Mou Leong Tan [1,*], Philip W. Gassman [2] and Arthur P. Cracknell [3]

[1] Department of Civil and Environmental Engineering, National University of Singapore, Singapore 117576, Singapore
[2] Center for Agricultural and Rural Development, Iowa State University, 560a Heady Hall, Ames, IA 20011-1054, USA; pwgassma@iastate.edu
[3] School of Engineering, Physics and Mathematics, University of Dundee, Dundee DDI 4HN, UK; apcracknell774787@yahoo.co.uk
* Correspondence: mouleong@gmail.com or ceetml@nus.edu.sg; Tel.: +65-6516-2179

Academic Editor: Karim Abbaspour
Received: 16 December 2016; Accepted: 14 March 2017; Published: 21 March 2017

Abstract: Gridded climate products (GCPs) provide a potential source for representing weather in remote, poor quality or short-term observation regions. The accuracy of three long-term GCPs (Asian Precipitation—Highly-Resolved Observational Data Integration towards Evaluation of Water Resources: APHRODITE, Precipitation Estimation from Remotely Sensed Information using Artificial Neural Network-Climate Data Record: PERSIANN-CDR and National Centers for Environmental Prediction Climate Forecast System Reanalysis: NCEP-CFSR) was analyzed for the Kelantan River Basin (KRB) and Johor River Basin (JRB) in Malaysia from 1983 to 2007. Then, these GCPs were used as inputs into calibrated Soil and Water Assessment Tool (SWAT) models, to assess their capability in simulating streamflow. The results show that the APHRODITE data performed the best in precipitation estimation, followed by the PERSIANN-CDR and NCEP-CFSR datasets. The NCEP-CFSR daily maximum temperature data exhibited a better correlation than the minimum temperature data. For streamflow simulations, the APHRODITE data resulted in strong results for both basins, while the NCEP-CFSR data showed unsatisfactory performance. In contrast, the PERSIANN-CDR data showed acceptable representation of observed streamflow in the KRB, but failed to track the JRB observed streamflow. The combination of the APHRODITE precipitation and NCEP-CFSR temperature data resulted in accurate streamflow simulations. The APHRODITE and PERSIANN-CDR data often underestimated the extreme precipitation and streamflow, while the NCEP-CFSR data produced dramatic overestimations. Therefore, a direct application of NCEP-CFSR data should be avoided in this region. We recommend the use of APHRODITE precipitation and NCEP-CFSR temperature data in modeling of Malaysian water resources.

Keywords: NCEP-CFSR; APHRODITE; PERSIANN-CDR; SWAT; precipitation; Malaysia; streamflow; tropical; river; extreme

1. Introduction

Precipitation is a major component of the water cycle and is also a key input to hydrological and ecohydrological models. Meanwhile, the water cycle is largely influenced by changes in regional temperature [1]. Therefore, long-term precipitation and temperature information are vital to study climate changes, forecast local precipitation variability and extreme events trend analysis. Despite this, acquisition of reliable precipitation and temperature data is still a challenging task, especially

in developing countries. Ground-based gauge collection is generally regarded as the most accurate precipitation and temperature acquisition approach. However, there is a sparse network of climate stations in many regions due to high installation, operation and maintenance costs, and low awareness of the importance of such information [2], resulting in the inability to capture precipitation and temperature information at sufficient spatial and temporal resolutions.

Gridded climate products (GCPs), which have been developed from modeled and satellite remotely sensed data sources, are potentially alternative sources of climate data for streamflow modeling and other applications, which feature advantages of uninterrupted regional coverage, and high spatial and temporal resolutions [3–5]. For instance, the National Centers for Environmental Prediction Climate Forecast System Reanalysis (NCEP-CFSR) [6] and the Asian Precipitation—Highly-Resolved Observational Data Integration towards Evaluation of Water Resources (APHRODITE) [7] are available globally at a daily time-scale for periods of more than 35 years. Recently, Ashouri et al. [8] developed a new daily time-scale high resolution satellite precipitation product, called the Precipitation Estimation from Remotely Sensed Information using Artificial Neural Network-Climate Data Record (PERSIANN-CDR), for long-term hydro-climatic studies. However, the reliability of these products in many regions is still not well known.

Many studies have validated the performance of GCPs at either global, regional or catchment scale [9–11]. Many of the studies reveal regional differences in GCP performance. For example, Tan et al. [12] reported underestimation of precipitation values by APHRODITE over Peninsular Malaysia, whereas Jamandre and Narisma [13] showed overestimation of the same product in the Philippines. Based on Fekete et al. [14], such differences are expected to be larger in tropical regions compared to temperate regions due to the high precipitation variability. In addition, GCPs are associated with various uncertainties and differences in terms of algorithms, sources, spatial and temporal resolutions [15]. These errors can propagate into streamflow modeling via water cycle processes [16,17].

Reliable climate data are essential for hydrological modeling because errors in climate inputs could lead to false model outputs. For example, an inappropriate model setup with inaccurate GCPs could result in a seemingly "good" model [18], that leads to wrong simulations and subsequent decisions. Therefore, a capability assessment of GCPs prior to applying them in a hydrological model is critical to understanding and reducing these errors. In tropical regions, the capability of GCPs for hydrological assessments have been evaluated in the upper Mara Catchment, Kenya [19]; Negro River Basin, Amazon [20]; Blue Nile River Basin [21]; and Adean watersheds [22]. Vu et al. [23] compared five GCPs in streamflow simulations of the Dak Bla River in Vietnam and concluded that APHRODITE performed the best in replicating daily streamflows. APHRODITE was also used successfully by Le and Sharif [24] to evaluate climate change impacts on streamflow in the Huang River Basin in Central Vietnam. Several studies found that NCEP-CFSR performed poorly for streamflow simulations studies conducted in tropical or sub-tropical regions [25–27]. However, Auerbach et al. [28] reported satisfactory streamflow simulations using NCEP-CFSR for two catchments in Puerto Rico. Zhu et al. [29] and Ashouri et al. [30] report that PERSIANN-CDR performed well when used in streamflow simulations of sub-tropical catchments in China and the United States, respectively. Most studies have only focused on the GCP precipitation data assessments; comparatively few studies have also assessed the accuracy of GCP temperature data [31]. To date, the assessment of suitability and accuracy of these newly developed GCPs in streamflow simulations is still limited in Malaysia.

The overall goal of this study is to investigate the performance of long-term GCPs relative to climate data inputs via streamflow simulations for two major basins in Malaysia. This is an extension of the previous study by Tan et al. [12] which evaluated the performance of different GCPs across the entire country of Malaysia, but did not incorporate streamflow analysis. The specific objectives here for the two study basins are: (1) to assess the accuracy of the APHRODITE, PERSIANN-CDR and NCEP-CFSR data for precipitation and temperature data retrieval from 1983 to 2007; (2) to evaluate the capability of these products for streamflow simulations using the Soil and Water Assessment

Tool (SWAT) ecohydrological model [32–36]; and (3) to analyze the suitability of the three GCPs for capturing extreme hydro-climatic events.

2. Study Area and Materials

2.1. Study Area

Two tropical basins, the Kelantan River Basin (KRB) and Johor River Basin (JRB), were selected as study areas in this study due to differences in size, land use, topography and data availability (Figure 1). The KRB (4° N~6° N, 101° E~103° E) drains an area of 12,134 km^2 in northeastern Peninsular Malaysia. The main channel of the Kelantan River extends a total distance of about 248 km, and flows northward into the South China Sea. In 1990, the primary land use/land cover in the KRB was tropical forest (84.9%), followed by rubber (9.9%), oil palm (4.5%), urban (0.5%) and paddy (0.2%). The basin elevation ranges from 8 m a.s.l in the western region to 2174 m a.s.l in the southwestern regions. The KRB is characterized by a tropical monsoon climate, with an average annual precipitation ≥2500 mm, most of which falls from November to January [37]. The average annual temperature of the basin is about 27.5 °C. The KRB is frequently affected by monsoon flood events during the northeast monsoon season.

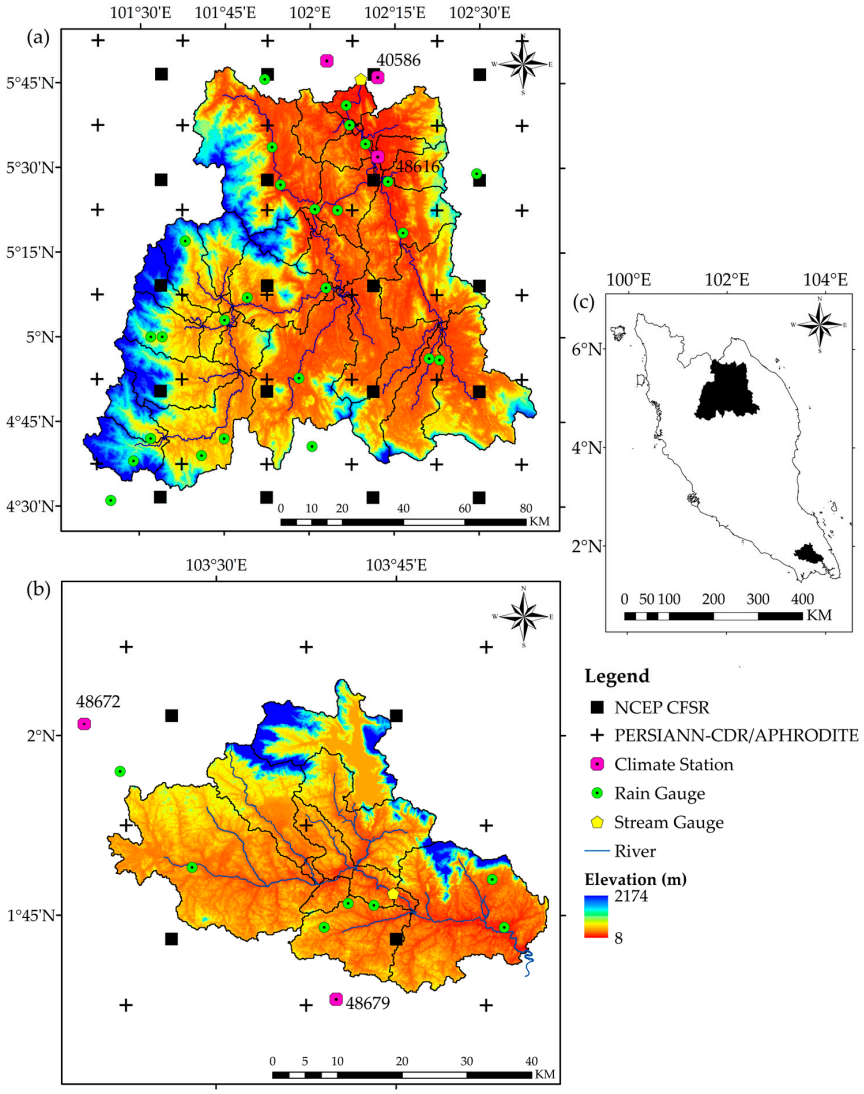

Figure 1. Spatial distribution of APHRODITE, PERSIANN-CDR, NCEP-CFSR and rain gauges over: (**a**) Kelantan River Basin (KRB); (**b**) Johor River Basin (JRB); and (**c**) Peninsular Malaysia.

The JRB (1° N~3° N, 103° E~104° E) drains an area of 1652 km^2 in southern Peninsular Malaysia (Figure 1b). The main river stem of the Johor River flows approximately 123 km southeast to the Strait of Johor. Elevations within the JRB range between 3 m a.s.l. and 977 m a.s.l, the highest elevations being located in the northern and western regions of the basin. The JRB is an agricultural production region, which is dominated by oil palm (38.4%), forest (44.1%) and rubber (15.3%) in 1990. The average annual precipitation and average annual temperature of the basin are 2500 mm and 26 °C, respectively. The Johor River is an important freshwater resource for the Johor and Singapore population, so any changes in water resources could lead to major impacts on agriculture, industrial and living conditions in both regions. For example, continuous hot weather in April 2016 resulted in water levels in the Linggiu Reservoir, located in the northern JRB falling to a new historic low.

2.2. Gridded Climate Products

Long-term GCPs are viable datasets that can be used for supporting the development of climate change and mitigation strategies for both the KRB and JRB. The evaluation of GCPs for this study focused on products characterized by long-term temporal climate datasets that contain data from at least a 30-year period. Based on this criterion, the APHRODITE, PERSIANN-CDR and NCEP-CFSR GCPs (Table 1) were assessed for the two study basins. Tan et al. [12] also reported that two Tropical Rainfall Measuring Mission (TRMM) 3B42 products performed well in replicating precipitation data for different sub-regions of Malaysia. However, the TRMM data were excluded from this study because the temporal resolution only extends back to 1998.

Table 1. Details on gridded climate products used in this study.

Name	Spatial	Temporal	Region	Sources
Rain Gauges				
Observation	Point	1983–present	Malaysia	Malaysia Meteorological Department; Department of Irrigation and Drainage Malaysia
Satellite				
PERSIANN-CDR	0.25°	1983–present	60° S–60° N	University of California, Irvine
Reanalysis data				
APHRODITE	0.25°	1951–2007	Eurasia	University of Tsukuba; Japan Meteorological Agency
NCEP-CFSR	0.3125°	1979–2014	Global	National Centers for Environmental Prediction

APHRODITE is a long-term daily precipitation product that spans the 57-year period of 1951 to 2007, which was generated from thousands of gauge observations data collected from various countries' government agencies [7]. It was developed by the Research Institute for Humanity and the Meteorological Research Institute of the Japan Meteorological Agency. APHRODITE is divided into Middle East, Russia, Monsoon Asia and Japan regions. In this study, APHRODITE V1101 (Monsoon Asia) with a 0.25° resolution was used.

PERSIANN-CDR provides daily precipitation information from 1983 to the present for latitudes 60° S–60° N at a spatial resolution of 0.25°. PERSIANN-CDR was established from the PERSIANN algorithm using Gridded Satellite Infrared Data (GridSat-B1), a calibrated and mapped geostationary satellite dataset [38]. The training of the artificial neural network is done using the NCEP stage IV hourly precipitation data. The product is then adjusted by the Global Precipitation Climatology Project (GPCP) monthly version 2.2 product [8].

NCEP-CFSR was constructed for a period of 36 years (1979 to 2014) at ~0.31° (38 km) resolution [6]. NCEP-CFSR is produced using cutting-edge data assimilation techniques and a forecast model that extrapolates non-observed parameters from observed data, collected from various sources such as rain gauges, ships, weather balloons and satellites. NCEP-CFSR data were obtained for the whole of Peninsular Malaysia (latitude 0.7° N–6.8° N and longitude 98.7° E–105.2° E), and then the stations

distributed over each basin were used. There are five climate parameters: temperature, precipitation, wind speed, relative humidity and solar radiation. However, the analysis conducted here was limited to just the NCEP-CFSR precipitation and temperature data, in order to maintain consistency with the evaluation of the other two GCPs.

2.3. Ground-Based Gauge Data

Daily precipitation, maximum temperature and minimum temperature data from 1983 to 2007 were collected from the Malaysia Meteorological Department (MMD; http://www.met.gov.my/) and the Irrigation and Drainage Department Malaysia (DID; http://www.water.gov.my/). There are 29 climate stations distributed across the KRB, but only three of them contain long-term maximum and minimum temperature data. For the JRB, daily precipitation data are available at nine climate stations. However, only two of the stations contain temperature data. In addition, monthly streamflow data measured at the Jambatan Guillermard and Rantau Panjang stations located in KRB and JRB (Figure 1), respectively, were collected from the DID for calibration and validation of the SWAT model. More detailed information of streamflow measurements for the KRB, JRB and other basins in Malaysia are available in a report prepared by DID [39].

2.4. Geospatial Data

The main input geospatial data for the SWAT model are a digital elevation model (DEM), a land use map and a soil map. Tan et al. [40] evaluated four different DEM datasets on SWAT simulations in the JRB, and found the 90 m Shuttle Radar Topography Mission (SRTM) DEM [41] performed the best. Therefore, the SRTM DEM was selected in this study. The land use map and soil map produced in 1990 and 2002, respectively, were obtained from the Ministry of Agriculture and Agro-based Industry of Malaysia (MOA; http://www.moa.gov.my/). In addition, the river network for each basin was digitized from the topography map produced by the Department of Survey and Mapping Malaysia (JUPEM; https://www.jupem.gov.my/). The digitized river networks were used to improve basin delineation and river extraction of both basins, especially in low land regions, similar to the approach used by Zheng et al. [42].

3. Methodology

3.1. Statistical Analysis

A set of continuous and categorical statistical analyses were used to evaluate the performance of the GCPs against observations at annual, seasonal, monthly and daily scales (Figure 1). As recommended by Tangang and Juneng [43], the climate data were divided into December to February (DJF), March to May (MAM), June to August (JJA) and September to November (SON) for seasonal scale assessment. The comparison was performed from 1983 to 2007 to provide a consistent time period, which brackets the starting year of 1983 for the PERSIANN-CDR dataset and the final year of 2007 for APHRODITE data. The point-to-pixel assessment was applied to prevent additional uncertainties during interpolation of the gauge data [44]. For the overall assessment, all precipitation values are pooled together from 1983 to 2007 [45]. In contrast, the NCEP-CFSR maximum and minimum temperature could not be validated at the overall assessment scale as there were only two or three climate stations that had temperature data in the KRB and JRB (Figure 1). Moreover, most of these stations are located outside the basins, and thus cannot be used to represent the entire basins. Therefore, the temperature data validation was conducted only for specific climate stations. In addition, the paired student *t*-test method was used to assess the significant differences between rain gauges and GCPs at the 0.05 significance level. Continuous statistical analysis such as Root Mean Square Error

(RMSE), Pearson Correlation Coefficient (CC), Mean Error (ME) and Relative Bias (RB) were used [12]. The formulas of these approaches are shown as follow:

$$\mathrm{RMSE} = \sqrt{\frac{\sum_{i=1}^{n} (G_i - O_i)^2}{n}} \quad (1)$$

$$\mathrm{CC} = \frac{\sum_{i=1}^{n} (O_i - \overline{O})(G_i - \overline{G})}{\sqrt{\sum_{i=1}^{n} (O_i - \overline{O})^2} . \sqrt{\sum_{i=1}^{n} (G_i - \overline{G})^2}} \quad (2)$$

$$\mathrm{ME} = \frac{\sum_{i=1}^{n} (G_i - O_i)}{n} \quad (3)$$

$$\mathrm{RB} = \frac{\sum_{i=1}^{n} (G_i - O_i)}{\sum_{i=1}^{n} O_i} (100) \quad (4)$$

where G_i and O_i are gridded and observed precipitation/temperature, respectively; i is used to label the individual measurements; and n is the number of measurements. CC measures similarity in temporal or spatial pattern between GCP and the observed data, RMSE evaluates the absolute average error between two datasets, ME makes it possible to evaluate the bias in estimations, while RB estimates the systematic overestimation and underestimation of GCP as a percentage (%). A good performance GCP should have a high CC, versus low RMSE, ME and RB values.

Categorical statistical analysis was used to evaluate the ability of GCPs to discriminate between precipitation and no precipitation event days, based on the following criteria [46]: (1) Accuracy (ACC), which represents the level of agreement between the GCPs and rain gauges estimates; (2) Probability of Detection (POD), which is a measure of how well the GCPs correctly detected rain gauge estimates; (3) False Alarm Ratio (FAR), which is used to evaluate how often the GCPs detected precipitation, but there was actually no precipitation recorded at the rain gauges; and (4) Critical Success Index (CSI), which is an indicator of the fraction of precipitation correctly detected by GCPs. These categorical approaches can be measured as follows:

$$\mathrm{ACC} = \frac{A + D}{n} \quad (5)$$

$$\mathrm{POD} = \frac{A}{A + C} \quad (6)$$

$$\mathrm{FAR} = \frac{B}{A + B} \quad (7)$$

$$\mathrm{CSI} = \frac{A}{A + B + C} \quad (8)$$

where A = correct detection (the GCP estimated precipitation, and precipitation was observed in rain gauge); B = false alarm (the GCP estimated precipitation, but precipitation was not observed in rain gauge); C = misses (the GCP did not estimate precipitation, but the rain gauge estimated precipitation); and D = correct negative (the GCP did not estimate precipitation, and precipitation was not observed in rain gauge). These values range between 0 and 1, where 1 is a perfect score for the ACC, POD and CSI, while 0 is a perfect score for the FAR. For example, the GCPs miss detecting the precipitation by 20%, if the FAR value is equal to 0.2. Further description of this approach is provided by Ebert et al. [46]. Based on Shen et al. [47], the quality of the GCP accuracy assessment is largely influenced by the

density and distribution of local station networks. Hence, assessment should be conducted over valid grid points only, where at least one station is available on each evaluated grid points.

3.2. SWAT Model

Current versions of the SWAT model represent more than three decades of model development at the co-located U.S. Department of Agriculture and Texas A&M University laboratories in Temple, Texas [34,35]. SWAT is usually executed at a daily time step for continuous simulations [36], typically with a minimum climatic dataset consisting of daily precipitation, maximum temperature and minimum temperature. The model has been applied for an extensive range of ecohydrological problems and scenarios worldwide for watershed scales ranging from <1 km^2 to entire continents (e.g., see reviews by Gassman et al. [48,49]; Bressiani et al. [25]; Gassman and Wang [50]; and Krysanova and White [51]). The model has also been used successfully for several hydrology and pollutant transport studies conducted in Malaysia [40,52–55]. SWAT version 2012 (Revision 635) was used in conjunction with the ArcSWAT interface version 2012.10_2.16 for this study.

In SWAT, a basin is usually first sub-divided into multiple sub-basins that are then further delineated into hydrologic response units (HRUs), which are smaller spatial units consisting of homogeneous soil, landscape, land use and management characteristics. HRUs represent a specific percentage of the corresponding sub-watershed area and are not currently spatially identified in SWAT. For this study, digitized stream networks were merged into the SRTM DEM using the "burn in" method, resulting in the delineation of 22 and 11 sub-basins for the KRB and JRB, respectively (Figure 1). Threshold values were then used in the ArcSWAT interface to create the HRUs, by setting minimum percentages that specific soils, slopes or land use had to occupy within a given sub-basin in order to be included in the KRB or JRB SWAT models. The hydrologic response unit (HRU) threshold values were defined as 20% for land use and slope, and 10% for soil, resulting in the KRB and JRB being further subdivided into 200 and 37 HRUs, respectively. Initial simulation of climate inputs, hydrological balance, crop growth and pollutant cycling occurs at the HRU level in SWAT. Excess discharge and pollutant exports are then aggregated across HRUs within a given sub-basin, input into the stream network at the sub-basin outlet and then ultimately routed to the watershed outlet. Further details regarding the theory, input requirements, and output options are provided in on-line documentation [33,36].

3.3. SWAT Model Baseline Testing

Baseline hydrological testing of SWAT was performed for both the KRB and JRB prior to the analysis of the GCPs. The respective baseline testing periods of 1983 to 1999 for the KRB and 1983 to 1992 for the JRB were based on streamflow data measured at the stream gauge sites shown for each basin in Figure 1. The first two years (1983–1984) were used as initialization years for both watersheds and the remainder of the time periods were subdivided into calibration (KRB = 1985–1994 and JRB = 1985–1988) and validation (KRB = 1995–1999 and JRB = 1989–1992) periods.

SWAT calibration was conducted using the Sequential Uncertainty Fitting algorithm (SUFI-2) within the SWAT Calibration and Uncertainty (SWAT-CUP) software package [56], which is a flexible algorithm that can process large numbers of input parameters. The Nash–Sutcliffe Coefficient (NSE) and Coefficient of Determination (R^2) statistics [57] were used to evaluate performance of simulated streamflow. The NSE was selected as the optimal objective in the SWAT calibration; NSE values can range from $-\infty$ to 1, where values ≤ 0 indicate that the mean of the measured data is a better predictor than the simulated values, indicating unacceptable performance. In addition, the R^2 values range from 0 to 1, and were used to assess the collinearity of the observed and simulated streamflow, where 1 is the ideal value. Based on Moriasi et al. [58,59], the performance of the SWAT model can be considered as satisfactory/good if the NSE and R^2 statistics are $\geq$0.5/0.7 and $\geq$0.6/0.75, respectively.

Following the SWAT calibration and validation phase, two different GCP scenarios were used as inputs into the calibrated SWAT model. The first scenario consisted of incorporating only the

precipitation data from the three GCPs into the SWAT model simulations. This allows comparison with several previous studies, which only evaluated the GCP precipitation products. The second scenario evaluated combinations of each GCP with the NCEP-CFSR temperature data (i.e., APHRODITE, PERSIANN-CDR or NCEP-CFSR precipitation data + NCEP-CFSR temperature) on the SWAT outputs. The second scenario is useful for assessing the applicability of the NCEP-CFSR temperature data in SWAT modeling, due to the sensitivity of the water cycle to temperature data.

3.4. Extreme Events Analysis

Extreme climatic events can result in severe impacts on human society and the environment [60]. The majority of existing hydrological and climatological studies, including analyses of the impacts of extreme climatic events have been conducted using ground-based gauge data [7,61]. Therefore, evaluation of other types of precipitation products for extreme events would provide important insight for determining their efficacy and accuracy for unusual climatic conditions [62]. Four indices were used in this study to assess the performance of the three GCPs in capturing the pattern of precipitation extremes over the KRB and JRB: (1) the number of precipitation days $\geq$10 mm·day^{-1} in a year (R10mm); (2) the number of precipitation days $\geq$50 mm·day^{-1} in a year (R50mm); (3) the annual maximum daily precipitation/streamflow amount(Rx1d); and (4) the annual maximum consecutive five-day precipitation/streamflow amount (Rx5d). The latter two indices were adopted to evaluate the accuracy of GCP-based SWAT simulated streamflows for maximum one-day and five-day amounts. These extreme indices were recommended by the Expert Team on Climate Change Detection and Indices [63]. Annual maximum one-day and five-day consecutive streamflow indices were chosen because these indices can be used to study flood volume which is important for flood risk management [29].

4. Results

4.1. Precipitation Validation

The result of the statistical assessment of the 25-year (1983 to 2007) comparisons between the APHRODITE, PERSIANN-CDR and NCEP-CFSR annual, seasonal, monthly and daily precipitation data versus the rain gauge observations for the KRB and JRB is listed in Table 2. The PERSIANN-CDR monthly-scale precipitation was the only GCP data that did not show significant differences relative to the KRB rain gauge observations, at a significance level of 0.05 (Table 2). The PERSIANN-CDR data showed insignificant differences versus observations at the JJA seasons in both basins.

In the KRB, the APHRODITE precipitation data produced the best linear correlation for all time-scales, with CC values varying from 0.38 to 0.74, followed by the PERSIANN-CDR and NCEP-CFSR data. It is also clear that the APHRODITE and PERSIANN-CDR precipitation data underestimated the annual, DJF, SON, monthly and daily precipitation amounts, based on the respective positive and negative signs for the ME and RB indicators, while the NCEP-CFSR data resulted in highly overestimated precipitation across the basin. In addition, the NCEP-CFSR data showed the largest average errors as evidenced by the highest RMSE values that ranged from 19.49 mm to 1695.34 mm for most of the time-scales, except for the DJF.

All other GCP data showed significant differences for annual, daily and monthly time steps as compared to the rain gauge precipitation estimates for the JRB (Table 2). The APHRODITE data produced the best results at the DJF, JJA, SON, monthly and daily time-scales, with CC values that ranged from 0.44 to 0.73. In contrast, the NCEP-CFSR data resulted in the worst performance at all time scales with CC values that spanned between 0.13 and 0.46. The APHRODITE data slightly underestimated the MMA, SON, monthly and daily precipitation levels, versus the PERSIANN-CDR and NCEP-CFSR data which produced large overestimations.

Generally, the GCPs show better linear correlation performance for the DJF and monthly time-scale estimations as compared to other time scales in both basins. The results found here showed that the

APHRODITE data produced the best precipitation estimation performance for over both basins, which is in agreement with Tan et al. [12] who conducted a national assessment over Malaysia. The main reason is due to the fact that the developers of APHRODITE incorporated MMD rain gauges' data in the development of the product [7]. On the contrary, NCEP-CFSR displays more serious errors and dramatically overestimated the total precipitation compared to the other GCPs. Similarly, Roth and Lemann [64] found that the total annual NCEP-CFSR precipitation data was three times greater than observed precipitation data in Ethiopia. The distinct weaknesses that have been quantified for the NCEP-CFSR data may be attributed to the scale differences, where the size of a grid point is huge (up to 0.3125°) compared to the station data which is a point-based measurement. The errors are expected to be higher in a grid point with high spatial and temporal variability of precipitation as well as for regions characterized by complex topography [65].

Table 2. Statistical analysis for daily, monthly, seasonal and annual precipitation in the Kelantan River Basin (KRB) and Johor River Basin (JRB). (Bold indicate significance at 0.05).

		KRB			JRB		
Time		**A**	**P**	**N**	**A**	**P**	**N**
Annual	RMSE (mm)	807.15	613.17	1695.34	399.51	514.77	1176.88
	CC	0.38	0.34	0.11	0.45	0.46	0.21
	ME (mm)	−540.53	−33.40	1314.21	−73.22	318.73	1018.59
	RB (%)	−20.51	−1.27	49.87	−3.21	13.96	44.61
	T test (*t* stat)	**20.40**	1.26	**31.21**	**2.09**	**8.65**	**23.15**
DJF	RMSE (mm)	334.13	288.09	333.39	191.87	232.70	406.94
	CC	0.63	0.62	0.48	0.73	0.71	0.36
	ME (mm)	−186.71	−78.86	41.40	4.54	119.62	275.76
	RB (%)	−27.96	−11.81	6.20	0.76	20.13	46.40
	T test (*t* stat)	**12.52**	**4.85**	**2.41**	0.19	**4.87**	**10.84**
MAM	RMSE (mm)	186.63	178.24	643.20	142.88	178.25	406.39
	CC	0.62	0.61	0.51	0.52	0.61	0.38
	ME (mm)	−80.90	52.10	523.70	−23.98	102.77	336.59
	RB (%)	−16.55	10.66	107.10	−4.02	17.23	56.41
	T test (*t* stat)	**8.47**	**5.49**	**29.15**	1.78	**6.60**	**17.88**
JJA	RMSE (mm)	212.59	184.19	499.33	127.20	157.30	246.20
	CC	0.44	0.35	0.20	0.66	0.35	0.16
	ME (mm)	−119.85	12.34	391.51	−27.24	−6.25	170.00
	RB (%)	−21.05	2.17	68.76	−5.59	−1.28	34.91
	T test (*t* stat)	**15.04**	1.57	**30.70**	**2.04**	0.50	**13.20**
SON	RMSE (mm)	310.21	269.49	552.17	153.81	192.77	334.56
	CC	0.58	0.57	0.21	0.44	0.42	0.13
	ME (mm)	−146.49	−13.54	367.27	−24.12	105.81	245.79
	RB (%)	−16.24	−1.50	40.71	−3.98	17.45	40.55
	T test (*t* stat)	**11.20**	0.97	**21.29**	1.86	**7.62**	**15.11**
Monthly	RMSE (mm)	126.98	118.62	210.02	78.15	93.86	149.75
	CC	0.74	0.72	0.48	0.71	0.64	0.46
	ME (mm)	−45.04	−2.78	109.52	−6.10	26.56	84.88
	RB (%)	−20.51	−1.27	49.87	−3.21	13.96	44.61
	T test (*t* stat)	**21.20**	1.24	**41.20**	**2.28**	**9.29**	**26.36**
Daily	RMSE (mm)	14.80	15.79	19.49	12.25	14.24	17.70
	CC	0.43	0.35	0.22	0.55	0.35	0.17
	ME (mm)	−1.48	−0.09	3.60	−0.20	0.87	2.79
	RB (%)	−20.51	−1.27	49.87	−3.22	13.96	44.60
	T test (*t* stat)	**41.93**	**2.47**	**85.44**	**3.30**	**14.57**	**41.80**
	Accuracy	0.61	0.57	0.55	0.67	0.55	0.49
	POD	0.87	0.86	0.94	0.89	0.89	0.96
	FAR	0.48	0.51	0.52	0.45	0.54	0.57
	CSI	0.48	0.45	0.46	0.51	0.44	0.42

Notes: A = APHRODITE; P = PERSIANN-CDR; N = NCEP-CFSR.

4.2. Precipitation Spatial Variability

The monthly CC and RB values for the GCPs over both basins are presented in Figures 2 and 3, respectively, to provide insights regarding spatial variability. Generally, high CC values for all GCPs were found for the northern and eastern KRB sub-regions, which are near coastal and low elevation areas (Figure 2a–c). All of the GCPs reflected strong performance of the CC values computed for the northwest JRB sub-region, while lower CC values dominated in the middle of the basin (Figure 2d–f). The APHRODITE data underestimated monthly ground-based precipitation at most of the stations (Figure 3). In contrast, the NCEP-CFSR data dramatically overestimated monthly precipitation at all of the stations, resulting in especially high RB values (more than 100%) for the stations mainly distributed in the southwestern KRB sub-region, which is characterized by high mountains (Figure 3c). The NCEP-CFSR was the only GCP which resulted in significant overestimates for all stations distributed across the JRB.

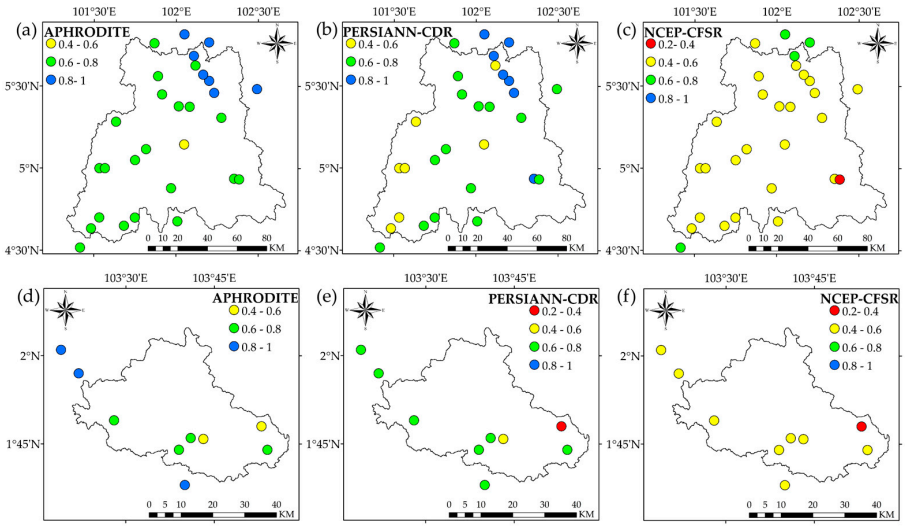

Figure 2. The correlation coefficient of monthly precipitation of APHRODITE, PERSIANN-CDR and NCEP-CFSR against rain gauges, respectively, over: (**a**–**c**) Kelantan River Basin; and (**d**–**f**) Johor River Basin.

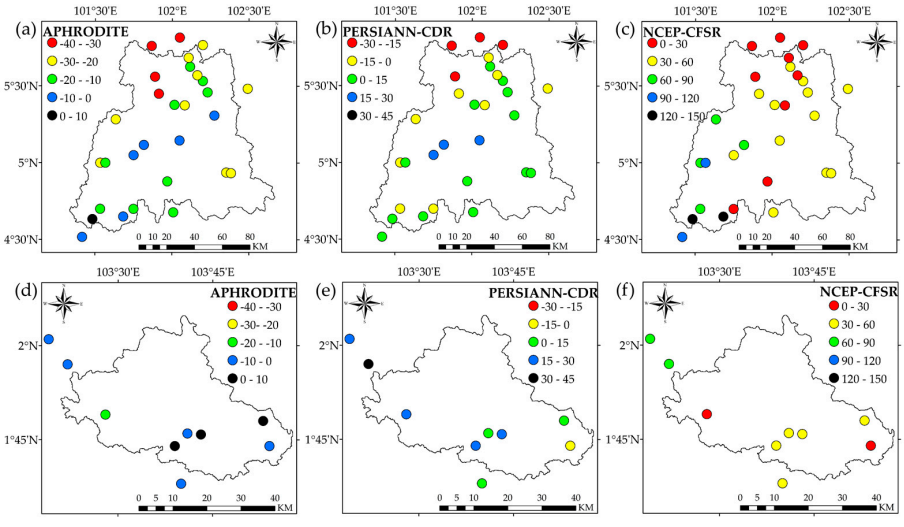

Figure 3. The relative bias of monthly precipitation of APHRODITE, PERSIANN-CDR and NCEP-CFSR against rain gauges, respectively, over: (**a**–**c**) Kelantan River Basin; and (**d**–**f**) Johor River Basin.

These findings agree with other studies, which state that GCPs generally are more reliable in low land regions compared to higher elevations [66,67]. This might be due to misrepresenting the effects of warm clouds, by infrared (IR) sensors that commonly appear on mountaintops [68]. The overall less accurate performance of GCPs in mountainous regions may be due to fewer rain gauges that can be used for product development. The installation and maintenance of climate stations in high mountainous regions is often problematic because of difficulties related to physical access and the fact the climate stations are representative of relatively small area due to high topography variability. In general, the APHRODITE dataset performed better for mountainous regions compared to other two GCPs, because the product has better orographic precipitation variability resolving skill [69].

4.3. Precipitation: Rain Detection and Intensity Assessment

The NCEP-CFSR data showed the most outstanding performance for rain detection ability assessment, with POD values of 0.94 and 0.96 for KRB and JRB, respectively. However, the APHRODITE exhibits better ACC skills for the JRB, indicating that it has a stronger capability to correctly estimate overall precipitation and non-precipitation events in southern Peninsular Malaysia. In contrast, the PERSIANN-CDR and NCEP-CFSR GCPs performed better for the KRB. The analysis further revealed that the NCEP-CFSR data were most prone to predicting false rain event, which in fact were not recorded by the rain gauges, resulting in the highest FAR values of 0.52 (KRB) and 0.57 (JRB). Moderate CSI values were also predicted for all three GCPs ranging from 0.45 to 0.48 (KRB) and 0.42 to 0.51 (JRB), demonstrating that roughly 50% of the precipitation was correctly estimated.

Figure 4 presents the probability distribution functions (PDFs) of precipitation intensity for the KRB and JRB. The non-precipitation values $\leq$0.254 mm·day^{-1} (common rain gauge threshold detection limit) were removed from the analysis. The three GCPs showed moderate underestimation for the $\geq$50 mm·day^{-1} precipitation classes over both basins. The NCEP-CFSR data resulted in significant overestimation for the 5–10 and 10–20 mm·day^{-1} precipitation classes in both basins. This is similar to the results reported by Blacutt et al. [70], who also discovered the NCEP-CFSR overestimated precipitation at 3–20 mm·day^{-1} class in Bolivia. They further reported the NCEP-CFSR tended to overestimate precipitation during the annual precipitation season period. This problem could potentially be amplified in both the KRB and JRB, which are typical tropical basins that receive precipitation throughout the year, especially during the northeast monsoon and southwest monsoon periods. The NCEP-CFSR data overestimation rate was higher for the JRB (up to 270% at 5–10 mm·day^{-1}) compared to the KRB, because the Sumatra and Titiwangsa mountain ranges help to reduce precipitation days in the KRB during the southwest monsoon season.

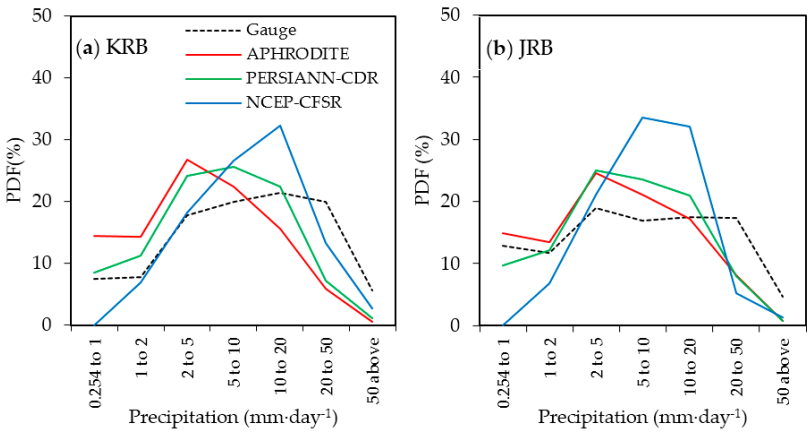

Figure 4. Probability distribution function (PDF) of daily precipitation from 1983 to 2007 from APHRODITE, PERSIANN-CDR, NCEP-CFSR and rain gauges over: (**a**) Kelantan River Basin (KRB); and (**b**) Johor River Basin (JRB).

4.4. Temperature Validation

The statistical analysis of the NCEP-CFSR maximum and minimum temperature versus climate stations temperature gauges (Figure 1) of the KRB and JRB is listed for various time scales in Table 3. The temperature values from each temperature gauge were compared to the nearest NCEP-CFSR grid point. Generally, the NCEP-CFSR temperature data have better correlation with observations at the DJF and monthly time-scale, with CC values ranging from 0.6 to 0.91 and 0.57 to 0.93, respectively. In addition, the daily maximum temperature data were better correlated with the observed data as compared to the minimum temperature data. However, the average error of the daily maximum temperature data (RMSE = 2.58 to 3.32 °C) is larger than the minimum temperature (RMSE = 0.98 to 2.68 °C) at all stations.

Box plots of the interactions between the NCEP-CFSR data and climate station maximum and minimum temperature data, for the four climate stations distributed across the KRB and JRB, are shown in Figure 5. The inter-quartile range shows that the minimum temperature at the 48679 station provides the best performance, as the range of the NCEP-CFSR data versus the gauge data matched quite well. The range of the NCEP-CFSR temperature data is larger than the observations at the all stations. As can be seen from the Table 3 and Figure 5, the NCEP-CFSR temperature data tend to underestimate the actual maximum and minimum temperature values. The main reason of the underestimation could be due to the land use types [65]. For example, the 48679 station is located in an industrial area where the surface temperature is expected to be higher. However, the NCEP-CFSR relies on National Aeronautics and Space Administration (NASA) land use information data [71], so reliable local land use information might be missing for the 48679 station location. Another possible reason for the underestimation of the NCEP-CFSR data may be explained by the mismatch of the temperature time measurement. For instance, the climate stations' daily maximum and minimum temperature data were taken at 0800 and 1400 local time, respectively, while the NCEP-CFSR daily maximum and minimum temperature were obtained from hourly values [72].

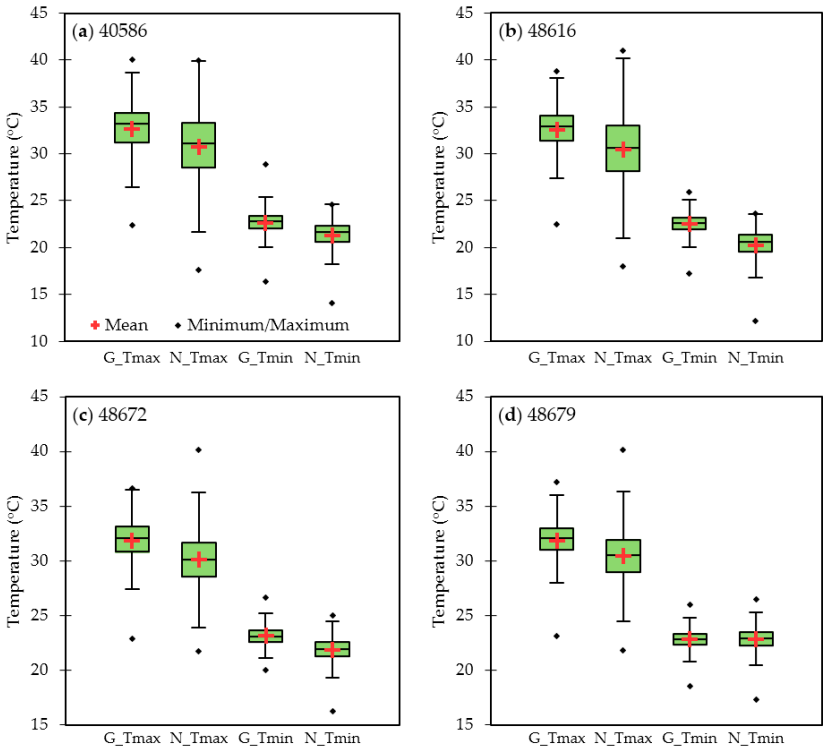

Figure 5. Box plots of daily maximum and minimum temperature derived from NCEP-CFSR (N) and temperature gauges (G) at: (**a**) 40586 station; (**b**) 48616 station; (**c**) 48672 station; and (**d**) 48679 station.

Table 3. Statistical analysis for the NCEP maximum (Tmax) and minimum (Tmin) temperature in the Kelantan River Basin and Johor River Basin.

Period		40586		48616		48672		48679	
		Tmax	Tmin	Tmax	Tmin	Tmax	Tmin	Tmax	Tmin
Annual	RMSE (°C)	1.97	1.37	2.22	2.31	1.74	1.28	1.49	0.18
	CC	0.74	0.82	0.43	0.62	0.72	0.81	0.53	0.84
	RB (%)	−5.81	−5.88	−6.43	−10.18	−5.27	−5.47	−4.36	0.22
DJF	RMSE (°C)	2.66	1.92	3.25	3.02	1.81	1.31	1.63	0.25
	CC	0.90	0.72	0.74	0.67	0.70	0.87	0.60	0.91
	RB (%)	−8.69	−8.53	−10.41	−13.65	−5.62	−5.63	−4.83	0.89
MAM	RMSE (°C)	2.02	1.46	2.25	2.63	2.12	1.26	1.82	0.20
	CC	0.90	0.48	0.71	0.25	0.81	0.67	0.75	0.84
	RB (%)	−5.66	−5.89	−5.92	−11.27	−5.95	−5.21	−4.83	−0.05
JJA	RMSE (°C)	1.19	1.12	1.30	1.83	1.57	1.64	1.38	0.30
	CC	0.45	0.70	0.07	0.63	0.65	0.55	0.27	0.59
	RB (%)	−2.64	−4.45	−2.65	−7.95	−4.69	−6.89	−3.99	0.14
SON	RMSE (°C)	2.26	1.19	2.43	1.86	1.64	0.99	1.37	0.23
	CC	0.42	0.51	0.38	0.54	0.62	0.70	0.51	0.80
	RB (%)	−6.62	−4.83	−7.20	−8.07	−4.84	−4.17	−3.88	−0.11
Monthly	RMSE (°C)	2.18	1.50	2.48	2.46	1.89	1.36	1.67	0.35
	CC	0.93	0.77	0.88	0.70	0.79	0.57	0.72	0.73
	RB (%)	−5.82	−5.90	−6.44	−10.21	−5.26	−5.48	−4.35	0.23
Daily	RMSE (°C)	2.96	1.80	3.32	2.68	2.77	1.67	2.58	0.98
	CC	0.74	0.60	0.68	0.53	0.55	0.28	0.50	0.38
	RB (%)	−5.81	−5.88	−6.43	−10.18	−5.27	−5.47	−4.36	0.22

4.5. Streamflow: GCPs Precipitation Data

Table 4 lists the best fitted calibration parameters for KRB and JRB. The calibration and validation of the SWAT model were conducted based on local knowledge and a literature review of the SWAT model in tropical regions (e.g., [54,55,73,74]). As can be seen in Table 4, the CN2 values were increased by 1% and 13% for the KRB and JRB, respectively. This increment of CN2 values was also observed in calibration of other tropical SWAT models [75–77]. The CN2 value was higher in the JRB as it is dominated by oil palm plantations, where the surface runoff is generally higher than in a forest basin (KRB). Generally, the SWAT simulations that were based on rain gauge data agreed well with the observed streamflow during the calibration and validation periods for both the KRB and JRB (Figure 6). The NSE values that were computed for the KRB (JRB) were 0.75 (0.78) and 0.65 (0.6) for the calibration and validation periods, respectively (Table 5), and the corresponding KRB (JRB) R^2 statistics were 0.87 (0.78) and 0.84 (0.61) indicating that the SWAT model performed well for both basins based on the previously discussed suggested criteria [58,59].

Table 4. Optimal calibration parameters for Kelantan River Basin (KRB) and Johor River Basin (JRB).

No.	Parameter Name	Parameter	Range		KRB	JRB
			Min	Max	Value	Value
1	groundwater "revap" coefficient	V_GW_REVAP	0.1	0.4	0.4	0.29
2	channel effective hydraulic conductivity	V_CH_K2	0	80	56.4	66.67
3	baseflow alpha factor	V_ALPHA_BF	0.1	0.5	0.12	0.14
4	initial SCS CN II value	R_CN2	0	0.35	0.1	0.13
5	groundwater delay	V_GW_DELAY	0	130	80.99	91
6	soil evaporation compensation factor	V_ESCO	0.4	0.9	0.52	0.42
7	threshold water depth in the shallow aquifer for flow	V_GWQMN	2200	4000	3940.6	3700
8	manning's value for main channel	V_CH_N2	0.2	0.3	0.28	0.24
9	available water capacity	R_SOL_AWC	0	0.5	0.25	0.35
10	surface runoff lag time	V_SURLAG	8	19	18.44	18.63
11	threshold depth of water in the shallow aquifer for "revap" to occur	V_REVAPMN	70	320	232.3	95
12	deep aquifer percolation faction	V_RCHRG_DP	0.4	0.6	0.52	0.58

Note: R indicates the default parameter value is multiplied by (1+ a given value) and V indicates the default parameter value is replaced with the given value.

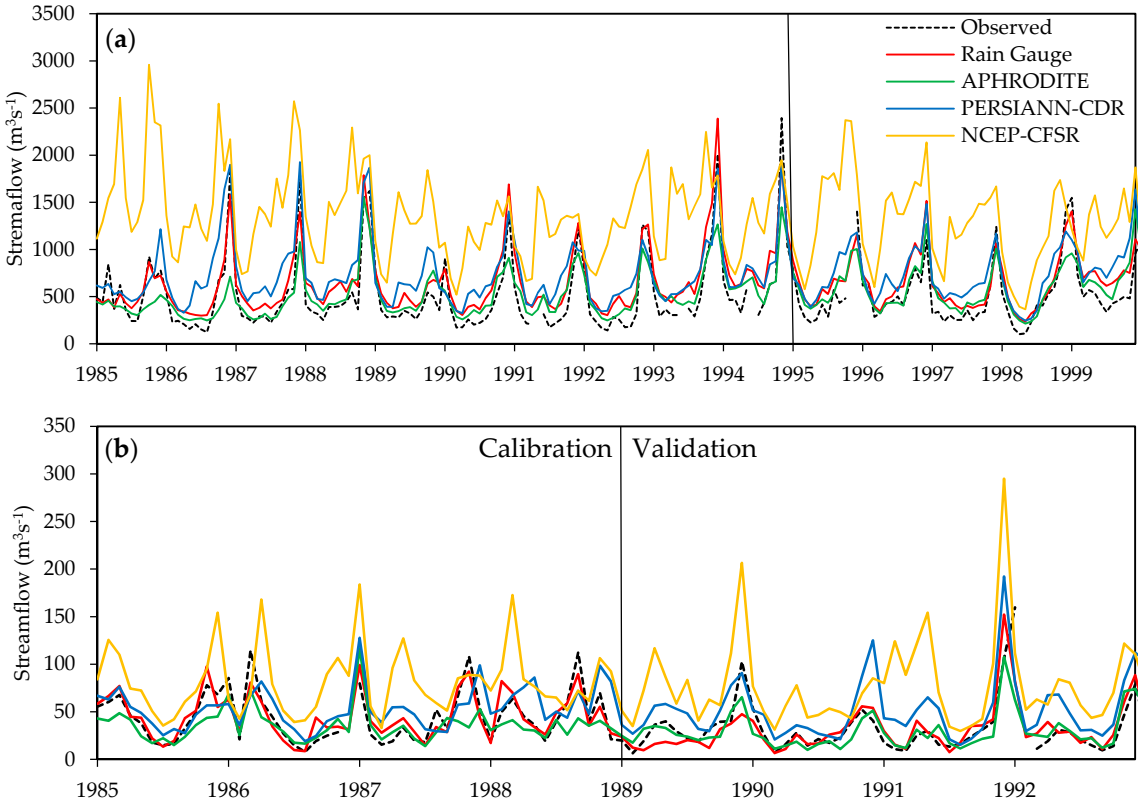

Figure 6. Comparison of observed streamflow with gauge-based, APHRODITE, PERSIANN-CDR and NCEP-CFSR precipitation-driven SWAT simulated monthly streamflow, respectively, in the: (**a**) Kelantan River Basin; and (**b**) Johor River Basin.

Table 5. SWAT calibration and validation statistical results for the Kelantan River Basin (KRB) and Johor River Basin (JRB).

Time		KRB	JRB
Calibration Period	R^2	0.87	0.78
	NSE	0.75	0.78
	RB	27.41	2.94
Validation Period	R^2	0.84	0.61
	NSE	0.65	0.60
	RB	26.57	−2.99

Among the three GCPs, the most accurate KRB SWAT simulations occurred in response to the APHRODITE precipitation input, followed by the simulations driven by the PERSIANN-CDR and NCEP-CFSR precipitation data. The SWAT simulation streamflow trends, based on the APHRODITE and PERSIANN-CDR data, revealed overestimation of low streamflows and underestimation of high streamflows. The predicted streamflow results obtained with the NCEP-CFSR data were unacceptable as reflected by the negative NSE values (Table 6). In addition, the NCEP-CFSR precipitation data resulted in relatively high overestimation of observed streamflows throughout the simulation period, as indicated by the high RB values of 167.77% and 143.72% during the calibration and validation periods, respectively.

Similar results were obtained in the JRB, where the SWAT simulations that were driven by the APHRODITE precipitation data yielded the best calibration and validation (Figure 6 and Table 6), followed again by the PERSIANN-CDR and NCEP-CFSR precipitation data. However, both the

PERSIANN-CDR and NCEP-CFSR data resulted in unacceptable performance as shown, by the mostly negative NSE values (Table 6). Overestimation of the observed streamflows is also clearly shown in the PERSIANN-CDR- and NCEP-CFSR-based JRB SWAT streamflow predictions (Figure 6b) by 57.63% and 142.45%, respectively, during the validation period (Table 6). However, the APHRODITE-based data tracked the observed streamflow well (Figure 6b), which was also confirmed by the majority of NSE, R^2 and RB statistics (Table 6), which indicated satisfactory results based on previously suggested criteria [58,59].

Table 6. Statistical analysis of GCPs performance in SWAT modeling in the Kelantan River Basin (KRB) and Johor River Basin (JRB).

		KRB			JRB		
		A	**P**	**N**	**A**	**P**	**N**
GCPs Precipitation							
Calibration Period	R^2	0.74	0.78	0.28	0.44	0.31	0.18
	NSE	0.69	0.49	−4.47	0.34	0.14	−2.39
	RB	0.40	43.01	167.77	−19.38	21.20	81.60
Validation Period	R^2	0.68	0.63	0.23	0.61	0.49	0.40
	NSE	0.64	0.15	−6.19	0.60	−0.11	−3.26
	RB	13.48	41.92	143.72	−9.36	57.63	142.45
GCPs Precipitation + NCEP-CFSR Temperature							
Calibration Period	R^2	0.75	0.78	0.28	0.44	0.32	0.17
	NSE	0.70	0.46	−4.60	0.35	0.10	−2.60
	RB	2.65	45.64	170.46	−18.39	24.26	84.88
Validation Period	R^2	0.69	0.64	0.23	0.61	0.49	0.40
	NSE	0.62	0.10	−6.40	0.61	−0.18	−3.43
	RB	15.43	44.18	146.30	−7.05	61.94	146.72

Notes: A = APHRODITE; P = PERSIANN-CDR; N = NCEP-CFSR.

4.6. Streamflow: GCPs Precipitation + NCEP-CFSR Temperature Data

The statistical indices (R^2, NSE and RB) are summarized in Table 6 for the SWAT simulations that were executed as a function of precipitation inputs from one of the three GCPs in combination with the NCEP-CFSR temperature data. The combinations of GCP precipitation inputs and NCEP-CFSR temperature data resulted in overestimations of the observed streamflow for the majority of the simulation period for both basins. Similarly, the most severe streamflow overpredictions resulted in response to the combination of NCEP-CFSR precipitation and NCEP-CFSR temperature data.

Generally, the integration of the NCEP-CFSR temperature data with the GCP precipitation data did not result in significant impacts on the SWAT simulations for either basin, compared to the simulations that were performed with just the GCP precipitation inputs. For example, the differences of the validation NSE values between the APHRODITE precipitation data input and the APHRODITE precipitation with the NCEP-CFSR temperature input for the KRB and JRB are 0.02 and 0.01, respectively. These findings show that the influence of the precipitation data on the local hydrological cycle is very dominant relative to the effects of the temperature data in this tropical region. This could be due to the small temperature range and variation that occurs in Malaysia as compared to more temperate or arid regions in other global sub-regions.

Some success was obtained by forcing the SWAT model with the integration of the APHRODITE precipitation and NCEP-CFSR temperature data. However, we could not ignore a tendency by the APHRODITE data to underestimate the actual precipitation, which in turn offset some of the trend in overestimated streamflow that occurred within the SWAT models in the two basins that we have studied. Based on Faramarzi et al. [18], inaccurate input data, wrong model structure and inappropriate model parameters could generate misleading SWAT model outputs. The input data error can easily be

identified using more reliable observations, while the other two require local expert knowledge with modeling skill. Hence, multiple GCP data should be evaluated through an initial assessment prior to applying them in any hydrological models.

4.7. Extreme Event Assessment

The final aspect of the overall analysis was to evaluate the capability of the GCPs to predict extreme precipitation events (Table 7). All of the GCPs showed significant differences at 0.05 significance level when compared with the observed precipitation, except for the NCEP-CFSR data when assessed for the Rx1d index for the KRB. The APHRODITE data exhibited better correlation with observed precipitation for three of the indices (Rx1d, Rx5d and R10mm) in both basins versus the other GCPs, while the PERSIANN-CDR data resulted in the best performance in the R50mm index estimation. In addition, the majority of the RB values, which were calculated for the Rx1d, Rx5d and R50mm indices estimated by the three GCPs, were negative. This is similar to the findings reported by Miao et al. [78], who found that the PERSIANN-CDR data tends to underestimate the Rx1d and Rx5d indices in the eastern China region. This can be explained by the fact that most of the GCPs underestimated the precipitation range which is greater than 50 mm in the two basins (Figure 4).

Table 7. Statistical analysis for extreme precipitation indices in Kelantan River Basin and Johor River Basin (bold indicate significance at 0.05).

		Kelantan River Basin			**Johor River Basin**		
Indices		**A**	**P**	**N**	**A**	**P**	**N**
Rx1d	RMSE (mm)	96.34	83.11	78.03	74.25	82.04	73.58
	CC	0.48	0.44	0.19	0.23	0.20	0.29
	ME (mm)	−70.00	−49.46	−3.01	−42.03	−56.58	15.41
	RB (%)	−54.47	−38.48	−2.34	−33.71	−45.38	12.36
	T test (*t* stat)	**23.98**	**16.31**	0.95	**9.24**	**11.69**	**2.70**
Rx5d	RMSE (mm)	176.86	150.29	157.23	95.92	99.56	139.09
	CC	0.62	0.53	0.21	0.57	0.39	0.18
	ME (mm)	−127.38	−74.32	−19.91	−53.27	−45.84	35.28
	RB (%)	−45.21	−26.37	−7.07	−24.03	−20.69	15.92
	T test (*t* stat)	**20.56**	**10.89**	**3.12**	**6.75**	**6.47**	**3.56**
R10mm	RMSE (days)	23.56	22.87	75.11	14.91	29.78	61.60
	CC	0.34	0.24	0.23	0.40	0.32	0.11
	ME (mm)	−13.33	11.05	64.57	5.42	24.74	55.78
	RB (%)	−16.79	13.92	81.32	8.07	36.81	83.00
	T test (*t* stat)	**15.15**	**13.11**	**30.43**	**4.60**	**13.56**	**30.66**
R50mm	RMSE (days)	9.38	7.97	7.67	6.58	6.56	5.64
	CC	0.40	0.45	−0.14	0.27	0.34	0.06
	ME (mm)	−7.90	−6.26	−1.19	−5.66	−5.67	−3.68
	RB (%)	−83.33	−66.08	−12.55	−70.76	−70.87	−46.08
	T test (*t* stat)	**36.00**	**27.18**	**4.51**	**12.55**	**23.30**	**12.55**

Notes: A = APHRODITE; P = PERSIANN-CDR; N = NCEP-CFSR.

The RB statistic was used to quantify the difference in accuracy in simulating extreme streamflow events, based on the Rx1d and Rx5d indices, between the rain gauge-based and other three GCPs for the KRB (Figure 7) and JRB (Figure 8) because it provided a reliable basis for comparison of different case studies [79]. The majority of the RB values calculated for the APHRODITE and PERSIANN-CDR Rx1d and Rx5d indices are negative, indicating that most of the high streamflows were underestimated. However, the reverse pattern can be observed for the RB values determined for the respective NCEP-CFSR indices, indicating that streamflow was significantly overestimated in both basins for the NCEP-CFSR-based SWAT simulations.

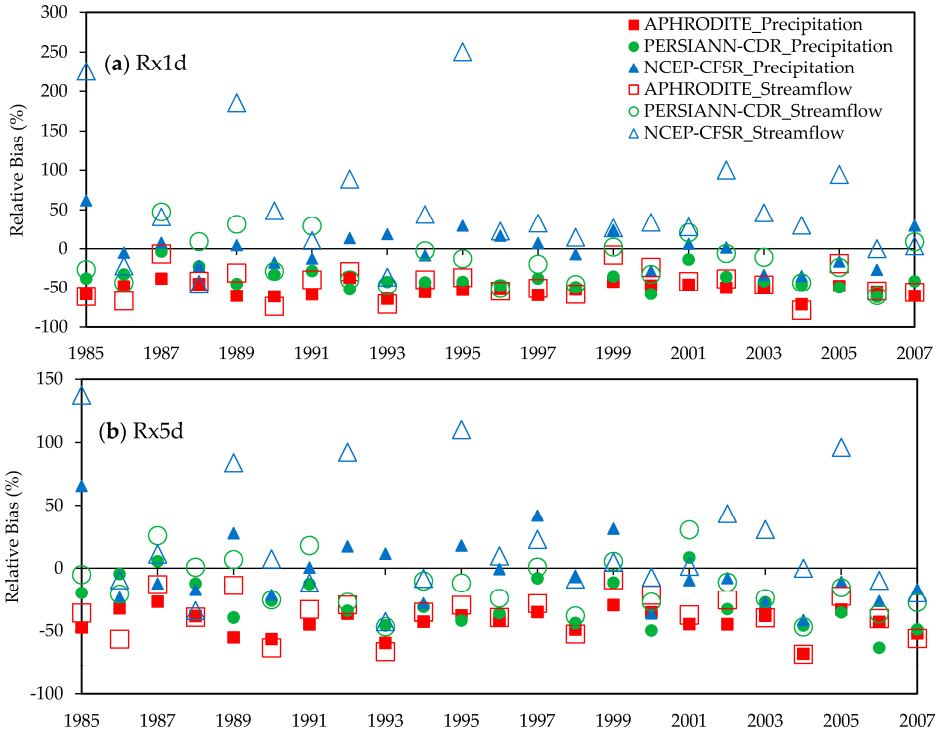

Figure 7. Relative bias values of annual maximum: (**a**) one-day precipitation/streamflow; and (**b**) five-day consecutive precipitation/streamflow from 1985 to 2007 in the Kelantan River Basin.

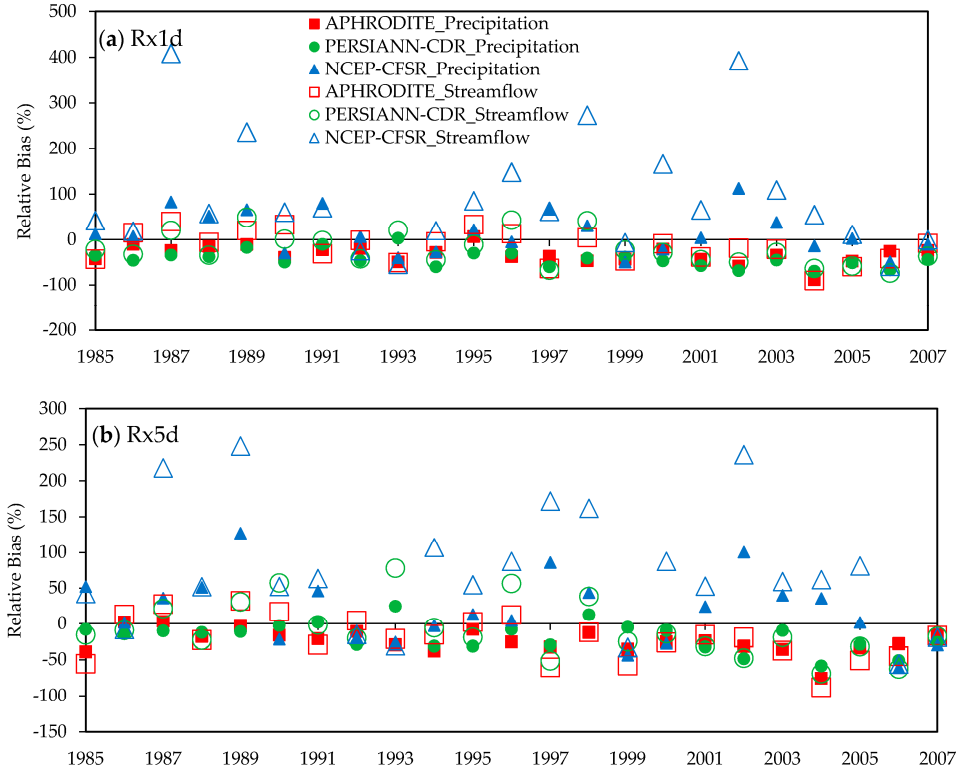

Figure 8. Relative bias values of annual maximum: (**a**) one-day precipitation/streamflow; and (**b**) five-day consecutive precipitation/streamflow from 1985 to 2007 in the Johor River Basin.

5. Discussion

In this study, six different sets of GCP precipitation and temperature inputs were forced to drive the SWAT model. The overall results of the analyses of the GCP data clearly revealed that the APHRODITE precipitation data resulted in the best performance of the three GCP data sources, based on the SWAT simulation graphical and statistical results. These results agree with the findings reported in several other studies, which showed that SWAT simulations executed with APHRODITE precipitation data performed very well in central Vietnam [23,24,80]; glacier influenced basins in mountainous regions in northwest China [81,82] and central Asia [83,84]; and a major tributary of the Yangtze River in central China [85]. Lauri et al. [31] also found that executing the VMod hydrological model [86] with combined APHRODITE precipitation and NCEP-CFSR temperature inputs accurately replicated hydrological simulations based on surface climate inputs of the 795,000 km^2 Mekong River Basin in southeast Asia. These composite results underscore the strength of the APHRODITE precipitation data for a variety of Asian conditions and that it can reliably be used for hydrological applications in un-gauged, data limited or restricted basins in the Southeast Asia.

The results found here clearly show that the original NCEP-CFSR precipitation is not suitable to apply for streamflow simulations in Malaysia, which is in agreement with the findings of Monteiro et al. [27], Roth and Lemann [64] and Bressiani et al. [87] for other tropical or sub-tropical conditions. However, the results found here conflict with the findings of Jajarmizadeh et al. [88], who report successful SWAT streamflow simulation results using the NCEP-CFSR data for the Roodan watershed that is located in southern Iran. Differences in climate and geographical conditions are the most likely explanation for such differences between the Jajarmizadeh et al. [88] study and the results reported in this research and other previously cited studies. In addition, the streamflow overestimation that resulted from the use of the NCEP-CFSR data in this study could be related to possible problems that occur over tropical regions [70], including the effects of the satellite algorithms on precipitation estimation and the CFSR model parameterizations.

In general, the performance of the APHRODITE data was better for the KRB compared to the JRB. This is due in part to a more complete distribution of rain gauges for the KRB versus the JRB (Figure 1); the JRB lacks long-term climate data representation in the northern part of the basin. In addition, the PERSIANN-CDR precipitation-based SWAT simulation also performed better for the KRB, which is consistent with Zhu et al. [29] who found that the PERSIANN-CDR data resulted in a smaller relative error in a data-rich region. These results are consistent with previously reported findings that improved SWAT hydrologic simulations usually occur in response to precipitation inputs characterized by higher resolution, versus lower resolution precipitation inputs [89–91].

As shown in Table 6, we also found that the effect of the basin size proved to be of minor importance compared to the performance of the three GCPs. For instance, the NCEP-CFSR data performed poorly in both basins, regardless of size and flow characteristics, while the APHRODITE precipitation resulted in the best performance for both basins. We also note that differences in sub-basin and/or HRU delineations, while not investigated in this study, typically do not impact SWAT streamflow and other hydrologic outputs as discussed in a previous review of SWAT literature [48] and reported in several subsequent SWAT applications [92–95].

Finally, it is important to emphasize that there were distinct periods within the overall simulation timeframe in which prevailing periods of bias actually were reversed for a specific GCP; e.g., streamflow extremes were overestimated during periods where precipitation extremes were underestimated. For example, the PERSIANN-CDR underestimated the Rx1d precipitation index by about 45% during 1989, but the corresponding Rx1d streamflow index was overestimated by 31.3%. This is consistent with the findings of a similar study conducted by Zhu et al. [29] for the Xiang River and Qu River watersheds in China. This finding indicates that there are certain periods where the precipitation generated by GCPs is unlikely to accurately capture the amount and durations of extreme events. This is further exacerbated by the fact that there is a variation between the precipitation and streamflow extremes temporal scales. For example, peak streamflow usually occurred a few days/hours after the

corresponding peak precipitation, but the peak streamflow normally represents an accumulation of precipitation events that occurred over several days/hours.

6. Conclusions

The performance of the APHRODITE, PERSIANN-CDR and NCEP-CFSR long-term gridded climate products (GCPs) were evaluated versus observed climate data for the Kelantan River Basin (KRB) and Johor River Basin (JRB), which are both tropical basins located in Peninsular Malaysia. The analysis included the assessment of capability of replicating streamflow for both basins using climate data from these GCPs as inputs to the calibrated SWAT model. The main conclusions obtained are as follows:

(1) The APHRODITE data typically replicated the observed monthly and daily precipitation more accurately over both the KRB and JRB, followed by the PERSIANN-CDR data and lastly the NCEP-CFSR data. The APHRODITE data tended to underestimate the observed daily and monthly precipitation in both basins, while the NCEP-CFSR data dramatically overestimated the observed precipitation data. The PERSIANN-CDR data resulted in a slight underestimation of the observed KRB precipitation and an overestimation of the JRB precipitation.

(2) The overall performance of the GCPs was better in low land and near coastal regions, such as the northern and eastern KRB. On the contrary, the performance of the GCPs was poor for the high mountainous regions located in the southwestern part of the KRB. Generally, the APHRODITE data resulted in stronger replication of precipitation in mountainous regions compared to the other two GCPs.

(3) The GCPs were found to have moderate accuracy (ACC), false alarm ratio (FAR), and critical success index (CSI), and a high probability of detection (POD) over the two basins that we have studied; the APHRODITE data resulted in the best performance. All three GCPs underestimated the extreme precipitation ranges ($\geq$50 mm·day^{-1}) and dramatically overestimated the observed moderate precipitation ranges (2–20 mm·day^{-1}).

(4) The APHRODITE data resulted in strong replication of observed streamflows when input to the calibrated SWAT simulations, while, the NCEP-CFSR was unable to replicate the observed streamflows for either basin in the calibrated SWAT. The PERSIANN-CDR data generated an in-between performance in the calibrated SWAT model, resulting in acceptable representation of KRB observed streamflows but an inability to track the JRB observed streamflows.

(5) We recommend the integration of the APHRODITE precipitation and the NCEP-CFSR temperature data for SWAT modeling in Malaysia as well as Southeast Asia region. However, a bias correction should be conducted if the gauge data are available, in order to improve the accuracy of the SWAT modeling.

(6) The APHRODITE data and PERSIANN-CDR data underestimated the annual maximum one-day streamflow (Rx1d) and five-day consecutive streamflow (Rx5d) indices. In contrast, the NCEP-CFSR dramatically overestimated the Rx1d and Rx5d streamflow indices in both basins. Basically, all three GCPs performed poorly in capturing extreme events, where high bias was found in certain periods.

Finally, these findings demonstrate how large uncertainties of GCP inputs can propagate within streamflow modeling, which can greatly affect the accuracy of streamflow simulations. This could lead to erroneous results that in turn could lead to wrong conclusions, which could impact the development of management systems and local policies. Therefore, development of an improved quantification framework for more accurate comparisons between different study areas should be a focus for future research. Similar studies should be conducted in other watershed systems with varying climatic and geographical conditions, to expand the testing of the GCPs and provide feedback to the GCP producers that can be used to develop better products.

Acknowledgments: This research was supported by the Ministry of Higher Education Malaysia and Universiti Teknologi Malaysia under the Transdisciplinary Research Grant Scheme (R.J130000.7809.4L835). The research was also funded in part from support received from the U.S. Department of Agriculture, National Institute of Food and Agriculture, Award No. 20116800230190, Climate Change, Mitigation, and Adaptation in Corn-Based Cropping Systems. We acknowledge Malaysian government agencies for providing the hydro-climatic and geographical data. Gratitude is also expressed to the original producers of the three global climate products for providing free downloadable data.

Author Contributions: Mou Leong Tan collected, processed and analyzed the data, and drafted the manuscript. Philip W. Gassman and Arthur P. Cracknell made contributions in reviewing and editing of the manuscript.

Conflicts of Interest: The authors declare no conflict of interest.

References

1. Held, I.M.; Soden, B.J. Robust responses of the hydrological cycle to global warming. *J. Clim.* **2006**, *19*, 5686–5699. [CrossRef]
2. Stokstad, E. Hydrology—Scarcity of rain, stream gages threatens forecasts. *Science* **1999**, *285*, 1199–1200. [CrossRef]
3. Abera, W.; Brocca, L.; Rigon, R. Comparative evaluation of different satellite rainfall estimation products and bias correction in the Upper Blue Nile (UBN) Basin. *Atmos. Res.* **2016**, *178–179*, 471–483. [CrossRef]
4. Yu, M.; Chen, X.; Li, L.; Bao, A.; Paix, M.L. Streamflow simulation by SWAT using different precipitation sources in large arid basins with scarce raingauges. *Water Resour. Manag.* **2011**, *25*, 2669–2681.
5. Gebremichael, M.; Bitew, M.M.; Hirpa, F.A.; Tesfay, G.N. Accuracy of satellite rainfall estimates in the Blue Nile Basin: Lowland plain versus highland mountain. *Water Resour. Res.* **2014**, *50*, 8775–8790.
6. Saha, S.; Moorthi, S.; Pan, H.-L.; Wu, X.; Wang, J.; Nadiga, S.; Tripp, P.; Kistler, R.; Woollen, J.; Behringer, D.; et al. The NCEP Climate Forecast System Reanalysis. *Bull. Am. Meteorol. Soc.* **2010**, *91*, 1015–1057. Available online: http://globalweather.tamu.edu (accessed on 21 March 2017).
7. Yatagai, A.; Kamiguchi, K.; Arakawa, O.; Hamada, A.; Yasutomi, N.; Kitoh, A. APHRODITE constructing a long-term daily gridded precipitation dataset for Asia based on a dense network of rain gauges. *Bull. Am. Meteorol. Soc.* **2012**, *93*, 1401–1415. Available online: http://www.chikyu.ac.jp/precip/english/products.html (accessed on 21 March 2017). [CrossRef]
8. Ashouri, H.; Hsu, K.-L.; Sorooshian, S.; Braithwaite, D.K.; Knapp, K.R.; Cecil, L.D.; Nelson, B.R.; Prat, O.P. PERSIANN-CDR: Daily precipitation climate data record from multi-satellite observations for hydrological and climate studies. *Bull. Am. Meteorol. Soc.* **2015**, *96*, 69–83. Available online: http://chrsdata.eng.uci.edu (accessed on 21 March 2017).
9. Dinku, T.; Ceccato, P.; Grover-Kopec, E.; Lemma, M.; Connor, S.J.; Ropelewski, C.F. Validation of satellite rainfall products over East Africa's complex topography. *Int. J. Remote Sens.* **2007**, *28*, 1503–1526. [CrossRef]
10. Wang, J.D.; Wang, W.Q.; Fu, X.H.; Seo, K.H. Tropical intraseasonal rainfall variability in the CFSR. *Clim. Dyn.* **2012**, *38*, 2191–2207.
11. Mashingia, F.; Mtalo, F.; Bruen, M. Validation of remotely sensed rainfall over major climatic regions in Northeast Tanzania. *Phys. Chem. Earth* **2014**, *67–69*, 55–63. [CrossRef]
12. Tan, M.L.; Ibrahim, A.L.; Duan, Z.; Cracknell, A.P.; Chaplot, V. Evaluation of six high-resolution satellite and ground-based precipitation products over Malaysia. *Remote Sens.* **2015**, *7*, 1504–1528. [CrossRef]
13. Jamandre, C.A.; Narisma, G.T. Spatio-temporal validation of satellite-based rainfall estimates in the Philippines. *Atmos. Res.* **2013**, *122*, 599–608. [CrossRef]
14. Fekete, B.M.; Vörösmarty, C.J.; Roads, J.O.; Willmott, C.J. Uncertainties in precipitation and their impacts on runoff estimates. *J. Clim.* **2004**, *17*, 294–304. [CrossRef]
15. Adler, R.F.; Huffman, G.J.; Chang, A.; Ferraro, R.; Xie, P.P.; Janowiak, J.; Rudolf, B.; Schneider, U.; Curtis, S.; Bolvin, D.; et al. The version-2 Global Precipitation Climatology Project (GPCP) monthly precipitation analysis (1979-present). *J. Hydrometeorol.* **2003**, *4*, 1147–1167.
16. Behrangi, A.; Khakbaz, B.; Jaw, T.C.; AghaKouchak, A.; Hsu, K.; Sorooshian, S. Hydrologic evaluation of satellite precipitation products over a mid-size basin. *J. Hydrol.* **2011**, *397*, 225–237. [CrossRef]
17. Seyyedi, H.; Anagnostou, E.N.; Beighley, E.; McCollum, J. Hydrologic evaluation of satellite and reanalysis precipitation datasets over a mid-latitude basin. *Atmos. Res.* **2015**, *164–165*, 37–48.

18. Faramarzi, M.; Srinivasan, R.; Iravani, M.; Bladon, K.D.; Abbaspour, K.C.; Zehnder, A.J.B.; Goss, G.G. Setting up a hydrological model of Alberta: Data discrimination analyses prior to calibration. *Environ. Model. Softw.* **2015**, *74*, 48–65.
19. Alemayehu, T.; van Griensven, A.; Bauwens, W. Evaluating CFSR and WATCH data as input to swat for the estimation of the potential evapotranspiration in a data-scarce Eastern-African catchment. *J. Hydrol. Eng.* **2016**, *21*, 16. [CrossRef]
20. Getirana, A.C.V.; Espinoza, J.C.V.; Ronchail, J.; Rotunno Filho, O.C. Assessment of different precipitation datasets and their impacts on the water balance of the Negro River Basin. *J. Hydrol.* **2011**, *404*, 304–322.
21. Dile, Y.T.; Srinivasan, R. Evaluation of CFSR climate data for hydrologic prediction in data-scarce watersheds: An application in the Blue Nile River Basin. *J. Am. Water Resour. Assoc.* **2014**, *50*, 1226–1241.
22. Strauch, M.; Kumar, R.; Eisner, S.; Mulligan, M.; Reinhardt, J.; Santini, W.; Vetter, T.; Friesen, J. Adjustment of global precipitation data for enhanced hydrologic modeling of tropical Andean Watersheds. *Clim. Chang.* **2016**, *141*, 547–560. [CrossRef]
23. Vu, M.T.; Raghavan, S.V.; Liong, S.Y. SWAT use of gridded observations for simulating runoff—A Vietnam river basin study. *Hydrol. Earth Syst. Sci.* **2012**, *16*, 2801–2811. [CrossRef]
24. Le, T.B.; Sharif, H.O. Modeling the projected changes of river flow in central Vietnam under different climate change scenarios. *Water* **2015**, *7*, 3579–3598.
25. Bressiani, D.D.; Gassman, P.W.; Fernandes, J.G.; Garbossa, L.H.P.; Srinivasan, R.; Bonuma, N.B.; Mendiondo, E.M. Review of Soil and Water Assessment Tool (SWAT) applications in Brazil: Challenges and prospects. *Int. J. Agric. Biol. Eng.* **2015**, *8*, 9–35.
26. Creech, C.T.; Siqueira, R.B.; Selegean, J.P.; Miller, C. Anthropogenic impacts to the sediment budget of São Francisco River navigation channel using SWAT. *Int. J. Agric. Biol. Eng.* **2015**, *8*, 140–157.
27. Monteiro, J.A.F.; Strauch, M.; Srinivasan, R.; Abbaspour, K.; Gucker, B. Accuracy of grid precipitation data for Brazil: Application in river discharge modelling of the Tocantins Catchment. *Hydrol. Process.* **2016**, *30*, 1419–1430. [CrossRef]
28. Auerbach, D.A.; Easton, Z.M.; Walter, M.T.; Flecker, A.S.; Fuka, D.R. Evaluating weather observations and the Climate Forecast System Reanalysis as inputs for hydrologic modelling in the tropics. *Hydrol. Process.* **2016**, *30*, 3466–3477. [CrossRef]
29. Zhu, Q.; Xuan, W.; Liu, L.; Xu, Y.-P. Evaluation and hydrological application of precipitation estimates derived from PERSIANN-CDR, TRMM 3B42V7, and NCEP-CFSR over humid regions in China. *Hydrol. Process.* **2016**, *30*, 3061–3083. [CrossRef]
30. Ashouri, H.; Nguyen, P.; Thorstensen, A.; Hsu, K.-L.; Sorooshian, S.; Braithwaite, D. Assessing the efficacy of high-resolution satellite-based PERSIANN-CDR precipitation product in simulating streamflow. *J. Hydrometeorol.* **2016**, *17*, 2061–2076. [CrossRef]
31. Lauri, H.; Rasanen, T.A.; Kummu, M. Using reanalysis and remotely sensed temperature and precipitation data for hydrological modeling in monsoon climate: Mekong river case study. *J. Hydrometeorol.* **2014**, *15*, 1532–1545. [CrossRef]
32. Arnold, J.G.; Srinivasan, R.; Muttiah, R.S.; Williams, J.R. Large area hydrologic modeling and assessment—Part 1: Model development. *J. Am. Water Resour. Assoc.* **1998**, *34*, 73–89. Available online: http://swat.tamu.edu/software/arcswat (accessed on 21 March 2017). [CrossRef]
33. Arnold, J.G.; Kiniry, J.R.; Srinivasan, R.; Williams, J.R.; Haney, E.B.; Neitsch, S.L. *Soil and Water Assessment Tool Input/Tool File Documentation. Version 2012*; Texas Water Resources Institute: College Station, TX, USA, 2012.
34. Arnold, J.G.; Moriasi, D.N.; Gassman, P.W.; Abbaspour, K.C.; White, M.J.; Srinivasan, R.; Santhi, C.; Harmel, R.D.; van Griensven, A.; van Liew, M.W.; et al. SWAT: Model use, calibration, and validation. *Trans. ASABE* **2012**, *55*, 1491–1508. [CrossRef]
35. Williams, J.R.; Arnold, J.G.; Kiniry, J.R.; Gassman, P.W.; Green, C.H. History of model development at Temple, Texas. *Hydrol. Sci. J.* **2008**, *53*, 948–960. [CrossRef]
36. Neitsch, S.L.; Arnold, J.G.; Kiniry, J.R.; Grassland, J.R.W. *Soil and Water Assessment Tool Theoretical Documentation Version 2009*; Agricultural Research Service Blackland Research Center: Temple, TX, USA, 2011.
37. Tan, M.L.; Ibrahim, A.L.; Cracknell, A.P.; Yusop, Z. Changes in precipitation extremes over the Kelantan River Basin, Malaysia. *Int. J. Climatol.* **2016**. [CrossRef]

38. Knapp, K.R.; Ansari, S.; Bain, C.L.; Bourassa, M.A.; Dickinson, M.J.; Funk, C.; Helms, C.N.; Hennon, C.C.; Holmes, C.D.; Huffman, G.J.; et al. Globally gridded satellite observations for climate studies. *Bull. Am. Meteorol. Soc.* **2011**, *92*, 893–907. [CrossRef]
39. Department of Irrigation and Drainage Malaysia (DID). *Hydrological Procedure No. 15: River Discharge Measurement by Current Meter*; DID: Kuala Lumpur, Malaysia, 1995.
40. Tan, M.L.; Ficklin, D.L.; Dixon, B.; Ibrahim, A.L.; Yusop, Z.; Chaplot, V. Impacts of DEM resolution, source, and resampling technique on SWAT-simulated streamflow. *Appl. Geogr.* **2015**, *63*, 357–368. [CrossRef]
41. Farr, T.G.; Rosen, P.A.; Caro, E.; Crippen, R.; Duren, R.; Hensley, S.; Kobrick, M.; Paller, M.; Rodriguez, E.; Roth, L.; et al. The Shuttle Radar Topography Mission. *Rev. Geophys.* **2007**, *45*, 75–79. [CrossRef]
42. Zheng, J.; Li, G.-Y.; Han, Z.-Z.; Meng, G.-X. Hydrological cycle simulation of an irrigation district based on a SWAT model. *Math. Comput. Model.* **2010**, *51*, 1312–1318. [CrossRef]
43. Tangang, F.T.; Juneng, L. Mechanisms of Malaysian rainfall anomalies. *J. Clim.* **2004**, *17*, 3616–3622.
44. Dembélé, M.; Zwart, S.J. Evaluation and comparison of satellite-based rainfall products in Burkina Faso, West Africa. *Int. J. Remote Sens.* **2016**, *37*, 3995–4014. [CrossRef]
45. Khan, S.I.; Hong, Y.; Gourley, J.J.; Khattak, M.U.K.; Yong, B.; Vergara, H.J. Evaluation of three high-resolution satellite precipitation estimates: Potential for monsoon monitoring over Pakistan. *Adv. Space Res.* **2014**, *54*, 670–684.
46. Ebert, E.E.; Janowiak, J.E.; Kidd, C. Comparison of near-real-time precipitation estimates from satellite observations and numerical models. *Bull. Am. Meteorol. Soc.* **2007**, *88*, 47–64.
47. Shen, Y.; Xiong, A.Y.; Wang, Y.; Xie, P.P. Performance of high-resolution satellite precipitation products over China. *J. Geophys. Res. Atmos.* **2010**, *115*, D2. [CrossRef]
48. Gassman, P.W.; Reyes, M.R.; Green, C.H.; Arnold, J.G. The Soil and Water Assessment Tool: Historical development, applications, and future research directions. *Trans. ASABE* **2007**, *50*, 1211–1250. [CrossRef]
49. Gassman, P.W.; Sadeghi, A.M.; Srinivasan, R. Applications of the swat model special section: Overview and insights. *J. Environ. Qual.* **2014**, *43*, 1–8. [CrossRef] [PubMed]
50. Gassman, P.W.; Wang, Y.K. Ijabe swat special issue: Innovative modeling solutions for water resource problems. *Int. J. Agric. Biol. Eng.* **2015**, *8*, 1–8.
51. Krysanova, V.; White, M. Advances in water resources assessment with SWAT—An overview. *Hydrol. Sci. J.* **2015**, *60*, 771–783. [CrossRef]
52. Hasan, Z.A.; Hamidon, N.; Yusof, M.S.; Ab Ghani, A. Flow and sediment yield simulations for Bukit Merah Reservoir Catchment, Malaysia: A case study. *Water Sci. Technol.* **2012**, *66*, 2170–2176. [PubMed]
53. Memarian, H.; Balasundram, S.K.; Abbaspour, K.C.; Talib, J.B.; Teh Boon Sung, C.; Sood, A.M. SWAT-based hydrological modelling of tropical land use scenarios. *Hydrol. Sci. J.* **2014**, *59*, 1808–1829. [CrossRef]
54. Tan, M.L.; Ficklin, D.L.; Ibrahim, A.L.; Yusop, Z. Impacts and uncertainties of climate change on streamflow of the Johor River Basin, Malaysia using a CMIP5 General Circulation Model ensemble. *J. Water Clim. Chang.* **2014**, *5*, 676–695.
55. Tan, M.L.; Ibrahim, A.L.; Yusop, Z.; Duan, Z.; Ling, L. Impacts of land-use and climate variability on hydrological components in the Johor River Basin, Malaysia. *Hydrol. Sci. J.* **2015**, *60*, 873–889. [CrossRef]
56. Abbaspour, K.C.; Rouholahnejad, E.; Vaghefi, S.; Srinivasan, R.; Yang, H.; Kløve, B. A continental-scale hydrology and water quality model for Europe: Calibration and uncertainty of a high-resolution large-scale SWAT model. *J. Hydrol.* **2015**, *524*, 733–752. [CrossRef]
57. Krause, P.; Boyle, D.P.; Bäse, F. Comparison of different efficiency criteria for hydrological model assessment. *Adv. Geosci.* **2005**, *5*, 89–97. [CrossRef]
58. Moriasi, D.N.; Arnold, J.G.; van Liew, M.W.; Binger, R.L.; Harmel, R.D.; Veith, T. Model evaluation guidelines for systematic quantification of accuracy in watershed simulations. *Trans. ASABE* **2007**, *50*, 885–900.
59. Moriasi, D.N.; Gitau, M.W.; Pai, N.; Daggupati, P. Hydrologic and water quality models: Performance measures and evaluation criteria. *Trans. ASABE* **2015**, *58*, 1763–1785.
60. Groisman, P.Y.; Knight, R.W.; Easterling, D.R.; Karl, T.R.; Hegerl, G.C.; Razuvaev, V.A.N. Trends in intense precipitation in the climate record. *J. Clim.* **2005**, *18*, 1326–1350.
61. Li, C.; Wang, R.; Ning, H.; Luo, Q. Changes in climate extremes and their impact on wheat yield in Tianshan mountains region, Northwest China. *Environ. Earth Sci.* **2016**, *75*, 1–13. [CrossRef]
62. Tan, M.L.; Tan, K.C.; Chua, V.P.; Chan, N.W. Evaluation of TRMM product for monitoring drought in the Kelantan River Basin, Malaysia. *Water* **2017**, *9*, 57. [CrossRef]

63. Karl, T.R.; Nicholls, N.; Ghazi, A. CLIVAR/GCOS/WMO workshop on indices and indicators for climate extremes workshop summary. *Clim. Chang.* **1999**, *42*, 3–7. [CrossRef]
64. Roth, V.; Lemann, T. Comparing CFSR and conventional weather data for discharge and soil loss modelling with SWAT in small catchments in the Ethiopian highlands. *Hydrol. Earth Syst. Sci.* **2016**, *20*, 921–934. [CrossRef]
65. Decker, M.; Brunke, M.A.; Wang, Z.; Sakaguchi, K.; Zeng, X.B.; Bosilovich, M.G. Evaluation of the reanalysis products from GSFC, NCEP, and ECMWF using flux tower observations. *J. Clim.* **2012**, *25*, 1916–1944. [CrossRef]
66. Derin, Y.; Yilmaz, K.K. Evaluation of multiple satellite-based precipitation products over complex topography. *J. Hydrometeorol.* **2014**, *15*, 1498–1516.
67. Sun, W.; Mu, X.; Song, X.; Wu, D.; Cheng, A.; Qiu, B. Changes in extreme temperature and precipitation events in the Loess Plateau (China) during 1960–2013 under global warming. *Atmos. Res.* **2016**, *168*, 33–48. [CrossRef]
68. Yilmaz, K.K.; Hogue, T.S.; Hsu, K.L.; Sorooshian, S.; Gupta, H.V.; Wagener, T. Intercomparison of rain gauge, radar, and satellite-based precipitation estimates with emphasis on hydrologic forecasting. *J. Hydrometeorol.* **2005**, *6*, 497–517. [CrossRef]
69. Krakauer, N.; Pradhanang, S.; Lakhankar, T.; Jha, A. Evaluating satellite products for precipitation estimation in mountain regions: A case study for Nepal. *Remote Sens.* **2013**, *5*, 4107–4123. [CrossRef]
70. Blacutt, L.A.; Herdies, D.L.; de Gonçalves, L.G.G.; Vila, D.A.; Andrade, M. Precipitation comparison for the CFSR, MERRA, TRMM3B42 and combined scheme datasets in Bolivia. *Atmos. Res.* **2015**, *163*, 117–131. [CrossRef]
71. Meng, J.; Yang, R.Q.; Wei, H.L.; Ek, M.; Gayno, G.; Xie, P.P.; Mitchell, K. The land surface analysis in the NCEP Climate Forecast System Reanalysis. *J. Hydrometeorol.* **2012**, *13*, 1621–1630. [CrossRef]
72. Fuka, D.R.; Walter, M.T.; MacAlister, C.; Degaetano, A.T.; Steenhuis, T.S.; Easton, Z.M. Using the Climate Forecast System Reanalysis as weather input data for watershed models. *Hydrol. Process.* **2014**, *28*, 5613–5623.
73. Nyeko, M. Hydrologic modelling of data scarce basin with SWAT model: Capabilities and limitations. *Water Resour. Manag.* **2014**, *29*, 81–94. [CrossRef]
74. Tan, M.L.; Ibrahim, A.L.; Yusop, Z.; Chua, V.P.; Chan, N.W. Climate change impacts under CMIP5 RCP scenarios on water resources of the Kelantan River Basin, Malaysia. *Atmos. Res.* **2017**, *189*, 1–10. [CrossRef]
75. Fukunaga, D.C.; Cecílio, R.A.; Zanetti, S.S.; Oliveira, L.T.; Caiado, M.A.C. Application of the SWAT hydrologic model to a tropical watershed at Brazil. *Catena* **2015**, *125*, 206–213. [CrossRef]
76. Pereira, D.R.; Martinez, M.A.; da Silva, D.D.; Pruski, F.F. Hydrological simulation in a basin of typical tropical climate and soil using the SWAT model part II: Simulation of hydrological variables and soil use scenarios. *J. Hydrol. Reg. Stud.* **2016**, *5*, 149–163. [CrossRef]
77. Yesuf, H.M.; Melesse, A.M.; Zeleke, G.; Alamirew, T. Streamflow prediction uncertainty analysis and verification of SWAT model in a tropical watershed. *Environ. Earth Sci.* **2016**, *75*, 806. [CrossRef]
78. Miao, C.; Ashouri, H.; Hsu, K.-L.; Sorooshian, S.; Duan, Q. Evaluation of the PERSIANN-CDR daily rainfall estimates in capturing the behavior of extreme precipitation events over China. *J. Hydrometeorol.* **2015**, *16*, 1387–1396. [CrossRef]
79. Schaefli, B.; Gupta, H.V. Do nash values have value? *Hydrol. Process.* **2007**, *21*, 2075–2080. [CrossRef]
80. Thom, V.; Khoi, D.; Linh, D. Using gridded rainfall products in simulating streamflow in a tropical catchment—A case study of the Srepok River Catchment, Vietnam. *J. Hydrol. Hydromech.* **2017**, *65*, 18–25. [CrossRef]
81. Wang, X.L.; Luo, Y.; Sun, L.; Zhang, Y.Q. Assessing the effects of precipitation and temperature changes on hydrological processes in a glacier-dominated catchment. *Hydrol. Process.* **2015**, *29*, 4830–4845.
82. Gan, R.; Zuo, Q.T. Assessing the digital filter method for base flow estimation in glacier melt dominated basins. *Hydrol. Process.* **2016**, *30*, 1367–1375.
83. Sidike, A.; Chen, X.; Liu, T.; Durdiev, K.; Huang, Y. Investigating alternative climate data sources for hydrological simulations in the upstream of the Amu Darya River. *Water* **2016**, *8*, 441. [CrossRef]
84. Ma, C.K.; Sun, L.; Liu, S.Y.; Shao, M.A.; Luo, Y. Impact of climate change on the streamflow in the glacierized Chu River Basin, Central Asia. *J. Arid Land* **2015**, *7*, 501–513. [CrossRef]

85. Xu, H.L.; Xu, C.Y.; Chen, S.D.; Chen, H. Similarity and difference of global reanalysis datasets (WFD and APHRODITE) in driving lumped and distributed hydrological models in a humid region of China. *J. Hydrol.* **2016**, *542*, 343–356. [CrossRef]
86. Lauri, H.; de Moel, H.; Ward, P.J.; Rasanen, T.A.; Keskinen, M.; Kummu, M. Future changes in Mekong River hydrology: Impact of climate change and reservoir operation on discharge. *Hydrol. Earth Syst. Sci.* **2012**, *16*, 4603–4619.
87. Bressiani, D.A.; Srinivasan, R.; Jones, C.A.; Mendiondo, E.M. Effects of spatial and temporal weather data resolutions on streamflow modeling of a semi-arid basin, Northeast Brazil. *Int. J. Agric. Biol. Eng.* **2015**, *8*, 125–139.
88. Jajarmizadeh, M.; Sidek, L.M.; Mirzai, M.; Alaghmand, S.; Harun, S.; Majid, M.R. Prediction of surface flow by forcing of Climate Forecast System Reanalysis data. *Water Resour. Manag.* **2016**, *30*, 2627–2640. [CrossRef]
89. Schilling, K.E.; Gassman, P.W.; Kling, C.L.; Campbell, T.; Jha, M.K.; Wolter, C.F.; Arnold, J.G. The potential for agricultural land use change to reduce flood risk in a large watershed. *Hydrol. Process.* **2014**, *28*, 3314–3325. [CrossRef]
90. Chaplot, V.; Saleh, A.; Jaynes, D.B. Effect of the accuracy of spatial rainfall information on the modeling of water, sediment, and NO_3-N loads at the watershed level. *J. Hydrol.* **2005**, *312*, 223–234. [CrossRef]
91. Moriasi, D.N.; Starks, P.J. Effects of the resolution of soil dataset and precipitation dataset on SWAT2005 streamflow calibration parameters and simulation accuracy. *J. Soil Water Conserv.* **2010**, *65*, 63–78. [CrossRef]
92. Rouhani, H.; Willems, P.; Feyen, J. Effect of watershed delineation and areal rainfall distribution on runoff prediction using the SWAT model. *Hydrol. Res.* **2009**, *40*, 505–519. [CrossRef]
93. Wang, Y.; Montas, H.J.; Brubaker, K.L.; Leisnham, P.T.; Shirmohammadi, A.; Chanse, V.; Rockler, A.K. Impact of spatial discretization of hydrologic models on spatial distribution of nonpoint source pollution hotspots. *J. Hydrol. Eng.* **2016**, *21*, 12. [CrossRef]
94. Her, Y.; Frankenberger, J.; Chaubey, I.; Srinivasan, R. Threshold effects in hru definition of the Soil and Water Assessment Tool. *Trans. ASABE* **2015**, *58*, 367–378.
95. Shen, Z.Y.; Chen, L.; Liao, Q.; Liu, R.M.; Huang, Q. A comprehensive study of the effect of GIS data on hydrology and non-point source pollution modeling. *Agric. Water Manag.* **2013**, *118*, 93–102. [CrossRef]